*Journal of Earth Science*, *Vol. 28*, *No. 5*, *p. 926–932*, *October 2017* *ISSN 1674-487X*
*Printed in China*
https://doi.org/10.1007/s12583-017-0802-0

# Lattice Boltzmann Simulation of $CO_2$ Transport in Kerogen Nanopores—An Evaluation of $CO_2$ Sequestration in Organic-Rich Shales

**Sherifa Cudjoe, Reza Barati***
*Department of Chemical & Petroleum Engineering*, *University of Kansas*, *Lawrence KS* 66045, *USA*
Sherifa Cudjoe: http://orcid.org/0000-0002-6703-0525; Reza Barati: http://orcid.org/0000-0002-1064-9562

**ABSTRACT: Organic-rich shale resources remain an important source of hydrocarbons considering their substantial contribution to crude oil and natural gas production around the world. Moreover, as part of mitigating the greenhouse gas effects due to the emissions of carbon dioxide ($CO_2$) gas, organic-rich shales are considered a possible alternate geologic storage. This is due to the adsorptive properties of organic kerogen and clay minerals within the shale matrix. Therefore, this research looks at evaluating the sequestration potential of carbon dioxide ($CO_2$) gas in kerogen nanopores with the use of the lattice Boltzmann method under varying experimental pressures and different pore sizes. Gas flow in micro/nano pores differ in hydrodynamics due to the dominant pore wall effects, as the mean free path ($\lambda$) of the gas molecules become comparable to the characteristic length ($H$) of the pores. In so doing, the traditional computational methods break down beyond the continuum region, and the lattice Boltzmann method (LBM) is employed. The lattice Boltzmann method is a mesoscopic numerical method for fluid system, where a unit of gas particles is assigned a discrete distribution function ($f$). The particles stream along defined lattice links and collide locally at the lattice sites to conserve mass and momentum. The effects of gas-wall collisions (Knudsen layer effects) is incorporated into the LBM through an effective-relaxation-time model, and the discontinuous velocity at the pore walls is resolved with a slip boundary condition. Above all, the time lag (slip effect) created by $CO_2$ gas molecules due to adsorption and desorption over a time period, and the surface diffusion as a result of the adsorption-gradient are captured by an adsorption isotherm and included in our LBM. Implementing the Langmuir adsorption isotherm at the pore walls for both $CO_2$ gas revealed the underlying flow mechanism for $CO_2$ gas in a typical kerogen nano-pore is dominated by the slip flow regime. Increasing the equilibrium pressure, increases the mass flux due to adsorption. On the other hand, an increase in the nano-pore size caused further increase in the mass flux due to free gas and that due to adsorbed gas. Thus, in the kerogen nano-pores, $CO_2$ gas molecules are more adsorptive indicating a possible multi-layer adsorption. Therefore, this study not only provides a clear understanding of the underlying flow mechanism of $CO_2$ in kerogen nano-pores, but also provides a potential alternative means to mitigate the greenhouse gas effect (GHG) by sequestering $CO_2$ in organic-rich shales.**
**KEY WORDS: kerogen, nanopores, lattice Boltzmann method, $CO_2$ sequestration, slip flow, Langmuir isotherm.**

## 0 INTRODUCTION

Organic-rich shale resources remain an important source of hydrocarbon (both oil and gas) in the United States and also serve as alternative geologic storage of $CO_2$ (Kang et al., 2011) but the underlying flow regime of $CO_2$ in the kerogen nanopores remain uncertain. Inorganic matrix (micro-pores), organic kerogen (nano-pores) and micro-fractures make up an organic-rich shale reservoir. Kerogen is a component of organic matter which serves as the precursor to natural gas and oil; after kerogen undergoes thermal maturity, pores ranging from 2 to 50 nm with an average pore size of 10 nm are left behind, although, this may vary from shale play to shale play (Fathi and Akkutlu, 2013). In 2014, the energy information administration (EIA) estimated shale gas production at 12.3 trillion cubic feet (Tcf) accounting for about 48% of total U.S. dry natural gas production and shale oil production in 2015 was estimated at 4.9 million barrels per day contributing to about 52% of total U.S. crude oil production (EIA, 2015). Although these unconventional resources remain increasingly promising, their full potential is yet to be thoroughly exploited due to their complex and multiscale heterogeneous nature, rendering it difficult to successfully characterize and develop.

Currently, organic-rich shales are characterized by elec-

*Corresponding author: rezab@ku.edu


Manuscript received May 20, 2017.
Manuscript accepted August 15, 2017.

Cudjoe, S., Barati, R., 2017. Lattice Boltzmann Simulation of $CO_2$ Transport in Kerogen Nanopores—An Evaluation of $CO_2$ Sequestration in Organic-Rich Shales. *Journal of Earth Science*, 28(5): 926–932. https://doi.org/10.1007/s12583-017-0802-0. http://en.earth-science.net

tron microscopy methods, including scanning electron microscopy (SEM) and focused ion beam-scanning electron microscopy (FIB-SEM). The SEM provides a 2-D visual observation of the pores, fractures and mineral variations, while the FIB-SEM provides the ability to iteratively mill and image a region of interest (ROI). The serial sectioning of the ROI by the FIB produces a stack of 2-D SEM images, which are reconstructed into a 3-D volume to observe the pore structure and pore connectivity on a nanoscale. From the reconstructed volume, characterization analyses such as porosity estimation, pore size distribution, kerogen volume fraction among others can be performed (Chen et al., 2015; Elgmati et al., 2011; Curtis et al., 2010; Sondergeld et al., 2010). On the other hand, the intrusion means of characterizing organic-rich shales, such as mercury injection capillary pressure (MICP), cannot be fully trusted due to the ultra-tight nature of the shales and poor pore connectivity. The intrusion methods inject non-wetting fluids (such as mercury) at high pressures to invade accessible pores, which might not give a clear picture of the in-situ pore connectivity and pore size distribution.

Primarily, these unconventional shale resources are developed by multi-fractured horizontal wells which only yield between 5%–10% of the original liquid hydrocarbon-in-place (Yu et al., 2016; Zuloaga-Molero et al., 2016; Gamadi et al., 2013; Wan, 2013). Increased initial production within the first few months from new wells is attributed mainly to the highly permeable fracture networks driven by pressure gradient. A steep decline then follows and levels off at much lower rates, sustained by the very slow diffusion of the liquid hydrocarbons from the matrix micro-pores and kerogen nano-pores into the stimulated reservoir volume (SRV) to be produced (Li et al., 2017; Yu et al., 2016; Gamadi et al., 2013). Thus, about 90% of the original liquid hydrocarbon is left unrecovered in the kerogen nanopores, which requires the implementation of enhanced oil recovery techniques other than the short-term drilling of new wells. Furthermore, due to the poor pore connectivity of the shale medium, and with diffusion as the main flow mechanism, a gas recovery technique will prove most beneficial. Several laboratory observations and numerical simulation studies have examined and affirmed the potential of gas injection in organic-rich shales and tight reservoirs (Yu et al., 2016; Fragoso et al., 2015; Wan and Sheng, 2015; Wan, 2013). Unlike continuous $CO_2$ injection, $CO_2$ huff-n-puff allows the injected gas to permeate into the shale medium beyond the SRV region and into the isolated kerogen pockets as well as matrix micro-pores during the soaking period. The injected $CO_2$ changes the oil composition through multiple contact and mass transfer resulting in oil swelling, decreased viscosity of the in-situ liquid hydrocarbon as well as reduced interfacial tension (IFT). All these effects culminate to increase the rate of liquid hydrocarbon to the wellbore (Li et al., 2017; Sheng, 2016; Yu et al., 2016; Zuloaga-Molero et al., 2016; Hawthorne et al., 2014; Gamadi et al., 2013; Green and Willhite, 1988).

Consequently, gaseous flow at microscopic scale are affected by the rarefaction effect due to the finite Knudsen number as such the Navier-Stokes equations breakdown (Guo and Shu, 2013). The rarefaction effect occurs when the mean free path of the gas is of the same order of magnitude as the channel size. Knudsen number ($Kn$), defined as the ratio of the mean free length ($\lambda$) to the characteristic length ($H$) of the pores. For $0.001<Kn<0.1$, the slip flow regime dominates the porous medium while the transition flow regime fall in the range of $0.1<Kn<10$, and free molecular flow at $Kn>10$. In effect, microscopic gas flow at the nanoscale, is dominated by the molecular level pore-wall effects such as Knudsen diffusion, surface diffusion, and slip flow, adding to the total mass flow rate (Ren et al., 2014; Fathi and Akkutlu, 2013; Kang et al., 2011). As such to fundamentally investigate the transport processes in organic-rich shales and also measure the transport properties, the lattice Boltzmann method has proved to be efficient (Chen et al., 2015; Ren et al., 2014; Zhang et al., 2014; Fathi and Akkutlu, 2013). Moreover, the underlying transport mechanism of $CO_2$ within the micro- and nano-pores are poorly understood. Very few studies cover the use of the lattice Boltzmann method (LBM) in organic-rich shales (Ren et al., 2014; Zhang et al., 2014; Fathi and Akkutlu, 2013) and so far, their works have been focused on methane ($CH_4$) gas. Even so, Zhang et al. (2014) does not include the pore-wall effects of gas molecules in the micro- and nano-pores in their model. In this study, we consider the kerogen nanopores to be composed of 100% $CO_2$, thus binary gas diffusion is neglected. In addition, the effect of prevailing pressures and geometry size on the transport coefficient and pore-wall effects of $CO_2$, either in a gaseous or liquid (supercritical) state in kerogen nano-pores will be extensively studied.

Hence, this project looks at implementing the LBM to evaluate the flow of $CO_2$ beyond continuum flow in kerogen nano-pores to capture the pore-wall effects and transport properties under different conditions. This will provide a clearer insight into the $CO_2$ huff-n-puff recovery method and its storage mechanism to mitigate greenhouse gas effect.

## 1 LATTICE BOLTZMANN METHOD (LBM)

The lattice Boltzmann method is a mesoscopic numerical method for fluid system used to solve the kinetic equations (e.g., the Boltzmann Equation). It is an improvement over the lattice gas cellular automata (LGCA) as it reduces statistical noise otherwise encountered with the LGCA by replacing Boolean variables (discrete particles) at a given node with distribution functions which undergo both collision and streaming steps locally. This makes the LBM flexible and suitable for parallel computing (Gabbana, 2015; Guo and Shu, 2013; Mohamad, 2011) and it maintains its efficiency in more complex geometries (e.g., porous media) (Wolf-Gladrow, 2005). Unlike traditional computational fluid dynamics (CFD), Navier-Stokes equations (NS), where mass, momentum and energy conservation equations are solved on discrete nodes, elements or volumes, the LBM replaces the fluid with fractious particles (Mohamad, 2011). Thus, the LBM does not consider individual particles (e.g., molecular dynamics (MD)), but rather the behavior of a collection of particles as a unit assigned the distribution function (Guo and Shu, 2013; Mohamad, 2011). The particles stream along defined lattice links and collide locally at the lattice sites; the number of lattice links may vary. Figure 1 shows a D2Q9 lattice, 2-dimensional in space with nine (9) speeds. Each population unit is assigned a lattice velocity denoted by $e_i$ where, the lattice sites, $i$=0, 1, 2, … 8, are numbered in a counter-clockwise direction and each lattice velocity ($e_i$) has $x$ and $y$ components.

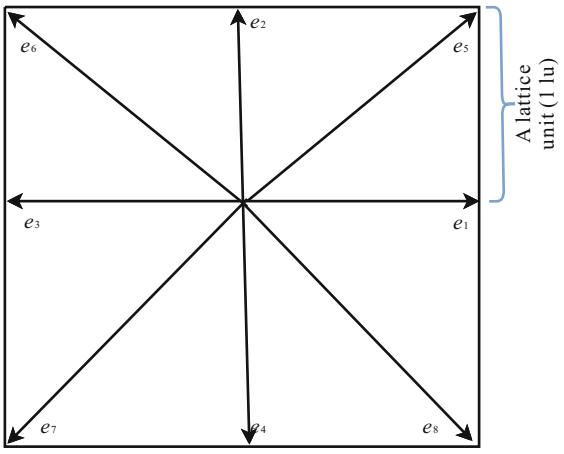


**Figure 1.** D2Q9 LBM with assigned lattice velocities (modified from Bao and Meskas, 2011).

The lattice velocities are scaled such that, for a given time interval ($\Delta t$), particles effectively move from exactly one cell to a neighboring cell and they are defined as (Bao and Meskas, 2011)

$$e_0 = (0, 0) \quad e_3 = (-1, 0) \quad e_6 = (-1, 1)$$
$$e_1 = (1, 0) \quad e_4 = (0, -1) \quad e_7 = (-1, -1)$$
$$e_2 = (0, 1) \quad e_5 = (1, 1) \quad e_8 = (1, -1)$$

The Boltzmann equation then describes the transportation of the distribution function ($f$) as (Guo and Shu, 2013)

$$\frac{\partial f}{\partial t} + u \cdot \nabla f = \Omega(f) \tag{1}$$

where $f$=distribution function, $u$=velocity, and $\Omega$=rate of change in due to binary molecular collisions. The distribution function ($f$) depends on the speed of the particles and not the time (Mohamad, 2011), as such, when the velocity distribution function ($f$) is obtained, the fluid density ($\rho$) and velocity ($u$) can be can be determined from its moments as (Guo and Shu, 2013)

$$\rho = \sum_i f_i \tag{2}$$

$$\rho u = \sum_i e_i f_i \tag{3}$$

The collision operator ($\Omega$) in the Boltzmann Equation is a bilinear integral function of the distribution function ($f$), and conserves mass, momentum, and energy. However, at equilibrium, the collision does not take net effects, as such the collision operator is approximated with simplified models, like the Bhatnagar- Gross-Krook (BGK) model (Guo and Shu, 2013; Bhatnagar et al., 1954)

$$\Omega_{\mathrm{BGK}} = -\frac{1}{\tau}[f - f^{\mathrm{eq}}] \tag{4}$$

where $\tau$=the relaxation time and $f^{\mathrm{eq}}$=the equilibrium distribution function. The BGK model reflects the overall effect of intermolecular collisions. The discrete equilibrium distribution function (EDF) can be expressed as (Guo and Shu, 2013)

$$f_i^{\mathrm{eq}} = \omega_i \rho \left[ 1 + \frac{e_i \cdot u}{c_s^2} + \frac{(e_i \cdot u)^2}{2c_s^4} - \frac{u^2}{2c_s^2} \right] \tag{5}$$

where $\omega_i$=weight associated with the velocity ($e_i$) and $c_s$=the speed of sound.

Table 1 gives the weight and speed of sound for the D2Q9 model assuming the lattice speed is 1. The first weight (4/9) corresponds to the particle at rest (0), the second weight (1/9) matches the four cardinal points, and the last weight (1/36) correlates with the intermediate directions.

**Table 1** Parameters of the D2Q9 model (Guo and Shu, 2013)

| Model | Weight ($\omega_i$) | $C_s^2$ |
|---|---|---|
| D2Q9 | 4/9, 1/9, 1/36 | 1/3 |

Therefore, intergrating Eq. (1) from $t$ to $t+\Delta t$ along the characteristic line and assuming a constant collision term, we obtain (Guo and Shu, 2013)

$$f_i(x+e_i\Delta t, t+\Delta t) - f_i(x,t) = -\frac{1}{\tau}\left[ f_i(x,t) - f_i^{\mathrm{eq}}(x,t) \right] \tag{6}$$

The macroscopic dynamics of a fluid can be inferred from the collective behavior of microscopic particles in the system, commonly described by the Navier-Stokes equations (NSE). The macroscopic NSE can be derived from the LBE under the Chapman-Enskog expansion, a multi-scale analysis developed by Chapman and Enskog (Guo and Shu, 2013). Therefore, the hydrodynamic equations corresponding to the D2Q9 model (Guo and Shu, 2013)

$$\frac{\partial \rho}{\partial t} + \nabla \cdot (\rho u) = 0 \tag{7}$$

$$\frac{\partial (\rho u)}{\partial t} + \nabla(\rho u u) = -\nabla p + \nabla \cdot [\rho \upsilon (\nabla u + \nabla u^T)] \tag{8}$$

where $\upsilon$=kinematic viscosity and is given by

$$\upsilon = c_s^2 \left( \tau - \frac{1}{2} \right) \Delta t \tag{9}$$

$u$=velocity, $\rho$=density, $t$=time, $p$=pressure, and $T$=transpose of directional velocity.

The LBGK models are deemed suitable for low speed flows due to the low Mach number assumption in the expansion of the discrete EDF from the Maxwellian distribution function (Guo and Shu, 2013). This makes the LBGK method an artificial compressibility method for incompressible NSE but several incompressible LBGK models have been developed to overcome the compressibility error from different view points (Guo and Shu, 2013).

On the other hand, the LBE method described above is mainly for macroscopic scales where the fluid is treated as a continuum. For flows of micro/nano origin, the hydrodynamics can differ in that some factors such as cohesive and adhesive forces, become dominant (Guo and Shu, 2013). Two main fundamental issues are considered in the application of LBE for micro gas flows: (1) relation between relaxation time and Knudsen number, and (2) slip boundary conditions.

### 1.1 Relation between Relaxation Time and Knudsen Number

From Eq. (9) the kinematic viscosity ($\upsilon$) is shown to depend on the relaxation time and from Chapman (1962), the relation between viscosity and the mean-free-path is given as

$$\lambda = \frac{\mu}{p}\sqrt{\frac{\pi RT}{2}} \tag{10}$$

Therefore, for a D2Q9 model of a flat wall (Fig. 2) below, the relationship between the relaxation time and $Kn$ can be established as (Guo and Shu, 2013)

$$\tau = \frac{1}{2} + \sqrt{\frac{6}{\pi}}\frac{Kn}{\Delta} \tag{11}$$

where $\ddot{A}=\Delta x/L$, $R$=gas constant, $T$=temperature, $L$= characteristic length, and $\Delta x$=height between a channel.

To incorporate the effects of gas-wall collisions (Knudsen layer effects), an effective-relaxation-time model is used as (Guo and Shu, 2013; Guo et al., 2007)

$$\lambda_e = \lambda\psi(Kn) \tag{12}$$

For a gas within a pore-slit (Fig. 2), $\psi$ is approximated as (Guo et al., 2007; Stops, 1970)

$$\psi(x) = \frac{2}{\pi}a\tan\left(\sqrt{2}x^{-3/4}\right) \tag{13}$$

Therefore, based on the relationship between the relaxation time and mean free path, an effective relaxation time with the gas-wall collision effect can be obtained as (Guo and Shu, 2013)

$$\tau = \left(\frac{\pi RT}{2}\right)^{-1/2}\lambda_e \tag{14}$$

### 1.2 Slip Boundary Condition

The velocity is discontinuous at the pore walls and to resolve this a slip boundary condition should be implemented. For a given pore-slit (Fig. 2) with a nanometer scale characteristic length, the half-way bounce-back/specular reflection (BSR) scheme can be applied at the boundary. The boundary is located at $j$=1/2 for a unidirectional flow. In the implementation of the LBE, the collision step (Eq. 15) is first carried out for all nodes, followed by the streaming step (Eq. 16) for all lattice points of $j$>1 respectively as (Guo and Shu, 2013)

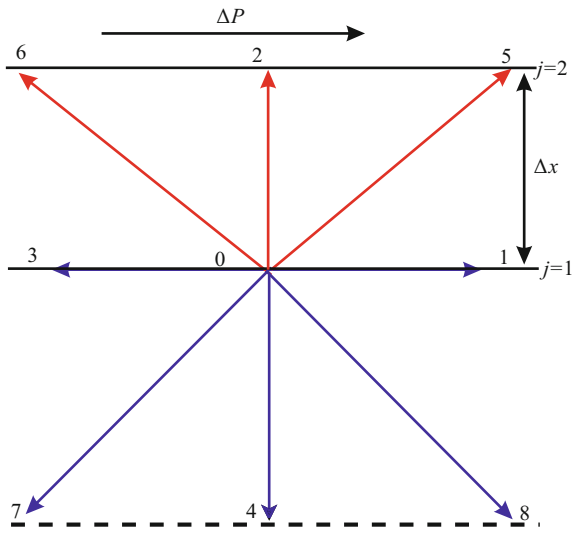


**Figure 2.** Lattice and boundary arrangement in D2Q9 model (modified from Guo and Shu, 2013).

$$f_i^{'} = f_i + \frac{1}{\tau}\left[f_i - f_i^{eq}\right] + \Delta t F_i \tag{15}$$

$$f_i(x + e_i\Delta t, t + \Delta t) = f_i^{'}(x,t) \tag{16}$$

where $f_i$=the forcing term. It may include the pressure gradient, gravity force or the interaction forces. The cohesive and adhesive forces between the gas molecules and the walls is covered by (Sukop and Or, 2004). The interaction forces are incorporated into the LBM from Newton's 2nd law with discrete representation of velocity and relaxation time, and using density as mass per unit area (Sukop and Or, 2004).

After streaming, the following distribution functions are known at the boundary ($j$=1): $f_0$, $f_1$, $f_3$, $f_7$, and $f_8$, while, $f_2$, $f_5$, and $f_8$ remain unknown but can be determined by the kinetic boundary condition (BSR) at the flat walls as (Guo and Shu, 2013)

$$\begin{aligned} f_2 &= f_4^{'} \\ f_5 &= rf_7^{'} + (1-r)f_8^{'} + 2r\rho\omega_5 e_5\cdot u_w / c_s^2 \\ f_6 &= rf_8^{'} + (1-r)f_7^{'} + 2r\rho\omega_6 e_6\cdot u_w / c_s^2 \end{aligned} \tag{17}$$

where, $r$=the bounce-back fraction required to take values in [0, 1] and $u_w$=the local wall velocity.

For some gas molecules such as $CO_2$, they are assumed to not just reflect at the pore-walls but rather adsorb and desorb at some time lag to cause an adsorption induced slip velocity (Fathi and Akkutlu, 2013; Chen and Tian, 2010). The surface diffusion as a result of adsorption-gradient is introduced into the LBM as a moving wall in the pore-slit and the slip velocity at every time step is calculated by the Langmuir isotherm equation (Ren et al., 2014; Fathi and Akkutlu, 2013; Chen and Tian, 2010). The wall velocity due to adsorbed-gas velocity in the $x$-direction is given as (Ren et al., 2015)

$$u_w = -D_{surf}\frac{\rho_s M}{\rho_{ads}V_{std}}\frac{q_L P_L}{(P_L + P)}\Delta P \tag{18}$$

where $D_{surf}$=surface diffusion coefficient, $\rho_s$=density of organic solid, $M$=$CO_2$ molecular weight, $V_{std}$=gas volume per mole at STP, $q_L$=Langmuir volume, $P_L$=Langmuir pressure, $P$=free-gas pressure, and $\Delta P$=pressure gradient.

Given the amount of adsorbed gas molecules at the solid surface as (Ren et al., 2014; Fathi and Akkutlu, 2013; Chen and Tian, 2010)

$$\alpha = \frac{V_L P}{P_L + P} \tag{19}$$

where $V_L$=the Langmuir volume parameter. Therefore, the slip velocity due to the pore-wall effects is given by (Ren et al., 2014; Fathi and Akkutlu, 2013; Chen and Tian, 2010)

$$u_{slip} = (1-\alpha)u_g + \alpha u_w \tag{20}$$

where $u_{slip}$=slip velocity and $u_g$=fluid velocity away from the wall

The LBE forms a second-order finite-difference (FD) scheme for the NSE and so considering a force-driven Poiseuille flow within a pore-slit, the analytical solution at the wall located at $y=L$ is given as (Guo and Shu, 2013)

$$u_j = 4u_a \frac{y_j}{H}\left[1-\frac{y_j}{L}\right]+u_s \tag{21}$$

where, $u_a = L^2(\Delta P)/8\upsilon$ and $u_s$=the slip velocity dependent on the boundary condition and with the relaxation time ($\tau$)–$Kn$ relationship, the slip velocity is expressed in terms of Kn as (Guo and Shu, 2013)

$$U_s = \frac{u_s}{u_a} = \frac{4(1-r)}{r}\sqrt{\frac{6}{\pi}}Kn + \frac{32}{\pi}Kn^2 - \Delta^2 \tag{22}$$

Thus, the slip velocity includes a first-order $Kn$ term, a second-order $Kn$ term, and grid-dependent term, and so for flows in slip regime, the linear part dominates, while the numerical part depends on the mesh size (Guo and Shu, 2013).

## 2 NUMERICAL SIMULATION

For the purposes of evaluating the pore-wall effects of $CO_2$ at different equilibrium pressures for $CO_2$ huff-n-puff and $CO_2$ sequestration, we considered a pore slit with characteristic length ranging from 10 nm and beyond at constant temperature. Input parameters for the numerical simulation were obtained from Nuttall's (2005) work on analyzing Devonian black shales in Kentucky for potential of $CO_2$ sequestration and enhanced fluid recovery. Table 2 reports on the amount of $CO_2$ adsorbed at varying pressures of 200 psi and 600 psi at an isotherm temperature of 86 ºF, in addition to the Langmuir parameters were made available (Nuttall, 2005). With a knowledge of the adsorbed thickness, the wall velocity due to adsorption-gradient can be estimated from Eq. (18) and consequently, the slip/Knudsen effect can be estimated from Eq. (20) at every time step with the LBE model. Figure 3 depicts the adsorbed phase (pink) and available space within the pore-slit for free gas flow and slip/Knudsen diffusion.

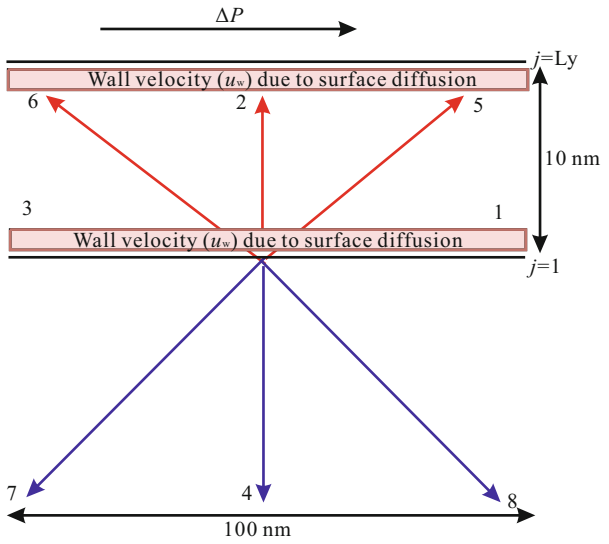


**Figure 3.** Schematic diagram of micro-gas flow in a pore-slit (modified from Ren et al., 2014).

## 3 RESULTS AND DISCUSSIONS

### 3.1 Evaluating $CO_2$ at Low Pressures for Potential Sequestration

At equilibrium pressures of 200 psi and 600 psi respectively, we simulated the properties of $CO_2$ gas within different geometries bearing in mind, the range of pores in kerogen nanopores (Curtis et al., 2010; Sondergeld et al., 2010). The following parameters given in Table 3 were observed and subsequently analyzed: the effect on slip velocity ($u_{slip}$), wall velocity (surface diffusion, $u_w$), the $Kn$, the free gas mass flux ($Q_{free}$) and the adsorbed-gas mass flux ($Q_{ads}$).

From Table 3 we can infer that, under the same prevailing conditions, $CO_2$ gas undergoes different flow regimes in a multi-scale heterogeneous system (e.g., organic-rich shales) based on the $Kn$. In other words, the interaction of $CO_2$ gas molecules with one another as well as with the walls are pronounced in kerogen nano-pores. Moreover, when $CO_2$ experiences transitional flow (Knudsen diffusion), the surface diffusion phenomenon becomes dominant as opposed to the slip flow effect. This is because in the transitional flow regime, the gas molecules interact with the walls more than with each other. This causes adsorbed gas molecules to desorb easily, hence increasing the surface diffusion phenomenon. On the other hand, the slip effect dominates $CO_2$ in the slip flow regime. Furthermore, the slip flow regime of the 20-nm pore slit records higher free gas mass flux than in the transition flow regime of the 10-nm pore silt. This goes to show that, the size of the nanopores geometry plays a significant role for gas to be adsorbed as well as free gas. The slip effect is the time lag between adsorption and desorption, and for a 20-nm pore slit, wider than a 10-nm pore-slit, the effect of slip would contribute to more free gas than for transitional flow regime in a thinner pore-slit.

The amount of adsorbed gas is on the same magnitude for both flow regimes, although the 20-nm pore-slit records a slightly higher value due to twice the available space for storage.

**Table 2** Summary of adsorption analysis for Ohio shale, 3 600–4 000 ft (Nuttall, 2005)

| Pressure | $CO_2$ adsorbed (scf/ton) | Langmuir parameters |
|---|---|---|
| 200 | 20.17 | $V_L$=37.5 ft$^3$/ton; $P_L$= 681.1 psia |
| 600 | 46.61 | Isotherm temperature=86 ºF |

**Table 3** Tabular results of LBM simulation at $P$=200 psi

| $P$ = 200 psi | | |
|---|---|---|
| | 10 (nm) pore slit | 20 (nm) pore slit |
| $Kn$ | 0.332 | 0.166 6 |
| $U_{slip}$ | 0.815 (μm/s) | 2.464 (μm/s) |
| $U_w$ | 1.121 (nm/s) | 1.229 (nm/s) |
| $Q_{free}$ | 200 (kg/m·s) | 1 248 (kg/m·s) |
| $Q_{ads}$ | 7.052 (μkg/m·s) | 7.734 (μkg/m·s) |

Figure 4 shows the velocity profile of the $CO_2$ gas in the 10-nm pore slit with the pore-wall effects at the boundary successfully captured.

Table 4 shows the LBM simulation carried out at a much higher pressure (600 psi) than the previous pressure. At a higher pressure, the dominant flow mechanism for $CO_2$ in kerogen nano-pores is the slip flow. Deducing from Table 4 below, in the slip flow regime, less $CO_2$ is adsorbed. On the other hand, Figure 5 shows very close match between the LB model and the analytical solution for slip flow regime.

Figure 5 shows a very close match between the LB model and the analytical solution for slip flow regime. The analytical solution deviates slightly from the wall nodes which points out its limitation.

One of the mechanisms of $CO_2$ sequestration often mentioned in literature is adsorption (Kang et al., 2011) and $CO_2$ gas clearly shows such tendencies. The linear shape of $CO_2$ allows the $CO_2$ molecules to come into contact more frequently than the spherically shaped methane (Tsai et al., 1985). In effect, the dispersion forces present between the $CO_2$ molecules become stronger and in effect enhances the adsorption potential.

**Table 4** Tabular results of LBM simulation at $P$=600 psi

| $P$=600 psi | | |
|---|---|---|
| | 10 (nm) pore slit | 20 (nm) pore slit |
| $Kn$ | 0.117 2 | 0.058 6 |
| $U_{slip}$ | 1.084 7 (μm/s) | 3.20 (μm/s) |
| $U_w$ | 2.103 7 (nm/s) | 2.411 0 (nm/s) |
| $Q_{free}$ | 266.3 (kg/m·s) | 1 320 (kg/m·s) |
| $Q_{ads}$ | 3.192 (μkg/m·s) | 3.658 6 (μkg/m·s) |

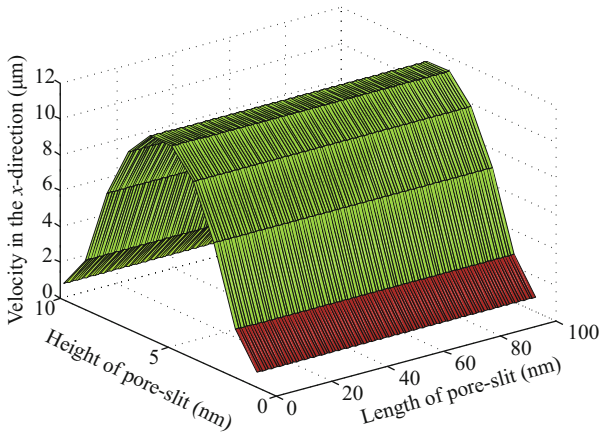


**Figure 4.** Velocity profile of $CO_2$ gas at 200 psi in 10 nm pore-slit.

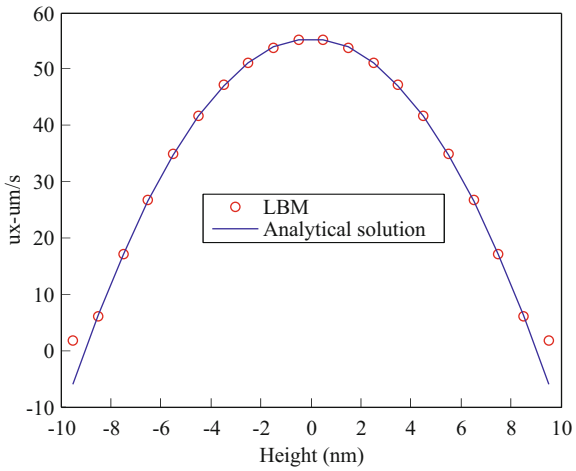


**Figure 5.** Validation of the LBM with the analytical solution.

### 3.2 $CO_2$ Enhanced Oil Recovery Potential

The injection of $CO_2$ into organic-rich shale to maximize liquid hydrocarbon recovery occurs at much higher pressures than the sequestration process. A change in flow regime was observed at the slightest increase in pressure under the sequestration process. As such, we would expect dominance of slip flow and to some extent, continuum flow to coexist in organic-rich shales during the $CO_2$ huff-n-puff process. Moreover, since, a dominant slip flow regime contributes to an increase in the free gas mass flux, we would expect the multiple contact miscibility and mass transfer purported to occur between the in-situ liquid hydrocarbon and the injected $CO_2$. This will eventually lead to the effects of oil swelling, reducing the liquid viscosity as well as the interfacial tension (IFT) reported in literature to cause an increase in oil flow rate.

## 4 CONCLUSION

Implementing correctly, the two fundamental points in micro-gas flow, successfully captures the dominant pore-wall effects. On the other hand, LBM simulation of $CO_2$ under different pressures and varying pore geometries gives a clear insight into the dominant flow regimes. This can also be incorporated into reservoir simulators to deduce further, the impact of the varying flow regimes on the sequestration and recovery of liquid hydrocarbon. Moreover, the free gas mass flux available for recovery in an organic-rich shale micro-/nano-pore varies directly with the characteristic length of the pore. This is inferred from the results, where a 20-nm pore slit at the same prevailing conditions as a 10-nm pore slit recorded higher free gas mass flux.

## ACKNOWLEDGMENT

Thanks go to the reviewers and the editors for their helpful suggestions. This work was made possible by the immense support of the Tertiary Oil Recovery Program (TORP) and the Kansas Interdisciplinary Carbonates Consortium (KICC) at the University of Kansas. The authors would like to thank both of these institutions for providing funding for this project. The final publication is available at Springer via https://doi.org/10.1007/s12583-017-0802-0.

## REFERENCES CITED

Bao, Y., Meskas, J., 2011. Lattice Boltzmann Method for Fluid Simulations. [2017-9-11]. http://www.math.nyu.edu/~billbao/report930.pdf

Bhatnagar, P. L., Gross, E. P., Krook, M., 1954. A Model for Collision Processes in Gases. I. Small Amplitude Processes in Charged and Neutral One-Component Systems. *Physical Review*, 94(3): 511–525. https://doi.org/10.1103/physrev.94.511

Chapman, S., 1962. The Mathematical Theory of Non-Uniform Gases. *American Journal of Physics*, 30(5): 389. https://doi.org/10.1119/1.1942035

Chen, L., Zhang, L., Kang, Q. J., et al., 2015. Nanoscale Simulation of Shale Transport Properties Using the Lattice Boltzmann Method: Permeability and Diffusivity. *Scientific Reports*, 5(1): 8089. https://doi.org/10.1038/srep08089

Chen, S., Tian, Z. W., 2010. Simulation of Thermal Micro-Flow Using Lattice Boltzmann Method with Langmuir Slip Model. *International Journal of Heat and Fluid Flow*, 31(2): 227–235. https://doi.org/10.1016/j.ijheatfluidflow.2009.12.006

Curtis, M. E., Ambrose, R. J., Sondergeld, C. H., 2010. Structural Characterization of Gas Shales on the Micro- and Nano-Scales. Canadian Unconventional Resources and International Petroleum Conference, Oct., 2010. 137693. https://doi.org/10.2118/137693-MS

EIA (Energy Information Administration), 2015. U.S. Crude Oil Production to 2025: Updated Projection of Crude Types. [2017-9-11] (2015-5-28). https://www.eia.gov/analysis/petroleum/crudetypes/

Elgmati, M., Zhang, H., Bai, B., et al., 2011. SPE 144050: Submicron-Pore Characterization of Shale Gas Plays. SPE North American Unconventional Conference and Exhibition. 1–19. https://doi.org/10.2118/144050-ms

Fathi, E., Akkutlu, I. Y., 2013. Lattice Boltzmann Method for Simulation of Shale Gas Transport in Kerogen. *Proceedings of SPE Annual Technical Conference and Exhibition*, 4(1): 27–37. https://doi.org/10.2118/146821-MS

Fragoso, A., Wang, Y., Jing, G., et al., 2015. Improving Recovery of Liquids from Shales through Gas Recycling and Dry Gas Injection. Society of Petroleum Engineers. [2017-9-11]. https://doi.org/10.2118/177278-MS

Gabbana, A., 2015. Accelerating the D3Q19 Lattice Boltzmann Model with OpenACC and MPI: [Dissertation]. Umeå University, Umeå

Gamadi, T. D., Sheng, J. J., Soliman, M. Y., 2013. An Experimental Study of Cyclic Gas Injection to Improve Shale Oil Recovery. SPE Annual Technical Conference and Exhibition. 1–9. [2017-09-11]. https://doi.org/10.2118/166334-MS

Green, D., Willhite, P., 1988. Enhanced Oil Recovery. 4th Ed. Richardson, Texas

Guo, Z. L., Shi, B. C., Zhao, T. S., et al., 2007. Discrete Effects on Boundary Conditions for the Lattice Boltzmann Equation in Simulating Microscale Gas Flows. *Physical Review E*, 76(5): 3–7. https://doi.org/10.1103/physreve.76.056704

Guo, Z., Shu, C., 2013. Lattice Boltzmann Method and Its applications in engineering. World Scientific Publishing (Vol. 3). World Scientif Publishing Co. Pte. Ltd., Singapore. https://doi.org/10.1142/8806

Hawthorne, S. B., Gorecki, C. D., Sorensen, J. A., et al., 2014. Hydrocarbon Mobilization Mechanisms Using $CO_2$ in an Unconventional Oil Play. *Energy Procedia*, 63: 7717–7723. https://doi.org/10.1016/j.egypro.2014.11.805

Kang, S. M., Fathi, E., Ambrose, R. J., et al., 2011. Carbon Dioxide Storage Capacity of Organic-Rich Shales. *SPE Journal*, 16(4): 842–855. https://doi.org/10.2118/134583-pa

Li, L., Sheng, J. J., Xu, J., 2017. SPE-185066-MS Gas Selection for Huff-n-Puff EOR in Shale Oil Reservoirs Based upon Experimental and Numerical Study. 1–15

Mohamad, A. A., 2011. Lattice Boltzmann Method Fundamentals and Engineering Applications with Computer Codes. Springer, New York. https://doi.org/10.1146/annurev.fluid.30.1.329

Nuttall, B. C., 2005. Analysis of Devonian Black Shales in Kenducky for Potential Carbon Dioxide Sequestration and Enhanced Natural Gas Production. Lexington, Kentucky. https://www.osti.gov/scitech/servlets/purl/842849

Ren, J. J., Guo, P., Guo, Z. L., et al., 2014. A Lattice Boltzmann Model for Simulating Gas Flow in Kerogen Pores. *Transport in Porous Media*, 106(2): 285–301. https://doi.org/10.1007/s11242-014-0401-9

Sheng, J., 2016. Maximize Liquid Oil Production from Shale Oil and Gas Condensate Reservoirs Synergy Opportunities. [2016-12-1]. https://www.netl.doe.gov/File Library/Events/2016/fy16 cs rd/Wed/Sheng.pdf

Sondergeld, C. H., Ambrose, R. J., Rai, C. S., et al., 2010. Micro-Structural Studies of Gas Shales. Society of Petroleum Engineers Unconventional Gas Conference, SPE Paper 131771. 17. https://doi.org/10.2118/131771-MS

Stops, D. W., 1970. The Mean Free Path of Gas Molecules in the Transition Regime. *Journal of Physics D*: *Applied Physics*, 3(5): 685–696. https://doi.org/10.1088/0022-3727/3/5/307

Sukop, M. C., Or, D., 2004. Lattice Boltzmann Method for Modeling Liquid-Vapor Interface Configurations in Porous Media. *Water Resources Research*, 40(1): 1–11. https://doi.org/10.1029/2003wr002333

Tsai, M. C., Chen, W. N., Cen, P. L., et al., 1985. Adsorption of Gas Mixture on Activated Carbon. *Carbon*, 23(2): 167–173. https://doi.org/10.1016/0008-6223(85)90008-9

Wan, T., 2013. Evaluation of the EOR Potential in Shale Oil Reservoirs by Cyclic Gas Injection. *Journal of Chemical Information and Modeling*, 53(9): 1689–1699. https://doi.org/10.1017/CBO9781107415324.004

Wan, T., Sheng, J. J., 2015. Evaluation of the EOR Potential in Hydraulically Fractured Shale Oil Reservoirs by Cyclic Gas Injection. *Petroleum Science and Technology*, 33(7): 812–818. https://doi.org/10.1080/10916466.2015.1010041

Wolf-Gladrow, D. A., 2005. Lattice-Gas Cellular Automata and Lattice Boltzmann Models—An Introduction. Springer, Bremerhaven. https://doi.org/978-3-540-66973-9

Yu, Y., Li, L., Sheng, J. J., 2016. SPE-181471-MS Further Discuss the Roles of Soaking Time and Pressure Depletion Rate in Gas Huff-n-Puff Process in Fractured Liquid-Rich Shale Reservoirs, April 2015, UAE: Society of Petroleum Engineers, Dubai. https://doi.org/10.2118/181471-MS. 1–17

Zhang, X. L., Xiao, L. Z., Shan, X. W., et al., 2014. Lattice Boltzmann Simulation of Shale Gas Transport in Organic Nano-Pores. *Scientific Reports*, 4(1): 4843. https://doi.org/10.1038/srep04843

Zuloaga-Molero, P., Yu, W., Xu, Y. F., et al., 2016. Simulation Study of $CO_2$-EOR in Tight Oil Reservoirs with Complex Fracture Geometries. *Scientific Reports*, 6(1): 33445. https://doi.org/10.1038/srep33445